Ultrafast Charge Transfer from CdSe Quantum Dots to p-Type NiO: Hole Injection vs Hole Trapping

ARTICLE *in* THE JOURNAL OF PHYSICAL CHEMISTRY C · JULY 2014

Impact Factor: 4.77 · DOI: 10.1021/jp506963q

THE JOURNAL OF PHYSICAL CHEMISTRY C

Article

pubs.acs.org/JPCC

Ultrafast Charge Transfer from CdSe Quantum Dots to p-Type NiO: Hole Injection vs Hole Trapping

Kaibo Zheng,*[,†] Karel Žídek,[†] Mohamed Abdellah,[†,§] Wei Zhang,[†] Pavel Chábera,[†] Nils Lenngren,[†] Arkady Yartsev,[†] and Tõnu Pullerits*[,†]

[†]Department of Chemical Physics, Lund University, Box 124, 22100, Lund, Sweden

[§]Department of Chemistry, Qena Faculty of Science, South Valley University, Qena 83523, Egypt

Supporting Information

ABSTRACT: Semiconductor quantum dot (QD) to metal oxide electron injection dynamics is well documented in the scientific literature. In contrast to that, not much is known so far about hole injection time scales in such systems. The current study fills this gap. We investigate photocathodes consisting of CdSe QDs and p-type NiO to study hole injection dynamics from the valence band of the QDs to NiO. The combination of two complementary techniques, ultrafast time-resolved absorption and fluorescence spectroscopies, enabled us to distinguish between hole trapping and injection. A kinetic component on the time scale of a few hundreds of picoseconds was identified as hole injection. By changing the size of the QDs, the driving force of the hole injection was tuned and we demonstrated that the hole injection rates are well described by the Marcus theory of charge transfer. In order to enhance the overall hole injection efficiency, we have passivated the CdSe QDs by a gradient ZnS shell. The core−shell QDs show significantly slower hole injection; still, since trapping was almost eliminated, the overall hole injection efficiency was greatly enhanced.

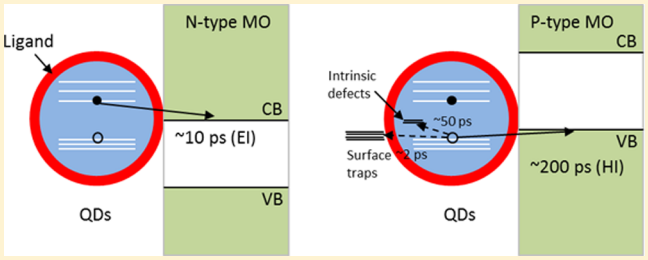

INTRODUCTION

Semiconductor quantum dots (QDs) are attractive as light-harvesting materials in photovoltaic applications due to their high extinction coefficient, their ability to generate multiple excitons, the size-dependent tunability of their bandgap, and their high stability.[1−7] In such solar cells, QDs are typically employed to form n-type photoanodes where photoexcited electrons are injected from the conduction band of QDs to n-type metal oxides.[8−10] On the other hand, when QDs are attached to hole acceptors, hole injection from the valence band of the QDs is expected if it is energetically favorable.[11,12] In this scenario, p-type photocathodes would be formed. Combining such photocathodes with photoanodes in a tandem configuration where anode and cathode materials absorb different spectral regions can significantly increase the efficiency of the device.[13]

Previous studies with conventional dye-sensitized solar cells (DSCs) have found that hole injection photocathodes are less efficient than electron transfer photoanodes. One reason is that hole injection competes with the fast recombination between the reduced dye and the holes generated in the nickel oxide (NiO).[14,15] It may be possible to solve the problem by replacing the dye molecules with semiconductor quantum dots, where the energy levels can be relatively easily tuned by controlling the QD size to facilitate the hole injection with optimal driving force. Recently, hole injection in p-type CdSe QD photocathodes was reported, providing incident photon-to-current conversion efficiencies up to 17%.[11] In order to take full use of QDs and optimize device performance, fundamental understanding of the ultrafast charge transfer dynamics is required. The following two questions need to be answered: (1) What is the pathway and time scale of hole injection in a p-type CdSe QD photocathode? (2) Can one optimize the hole injection by tuning the QD size?

Compared with the electron injection process in QD photoanodes, the hole injection is more complex due to numerous hole trapping pathways induced by surface defects and ligand groups.[16,17] In addition, the valence band (VB) dependence on CdSe QD size is different from the size dependence of the conduction band (CB). Consequently, the QD size dependence of the hole and electron injection driving forces can be very different.[18] Therefore, the conventional analysis strategy of electron dynamics needs to be modified to account for the specifics of hole injection.[19,20]

The article is organized as follows. First, we give an overview of the sample preparation and characterization procedures followed by a description of the time-resolved experimental setups. In the following section, we provide a thorough analysis of the hole trapping dynamics in CdSe QDs. This information is used to separate the hole injection dynamics from hole trapping. Then, the hole trapping from QDs with different sizes is studied and a theoretical description of the process is

Received: July 12, 2014
Revised: July 17, 2014
Published: July 21, 2014

   dx.doi.org/10.1021/jp506963q | J. Phys. Chem. C 2014, 118, 18462−18471

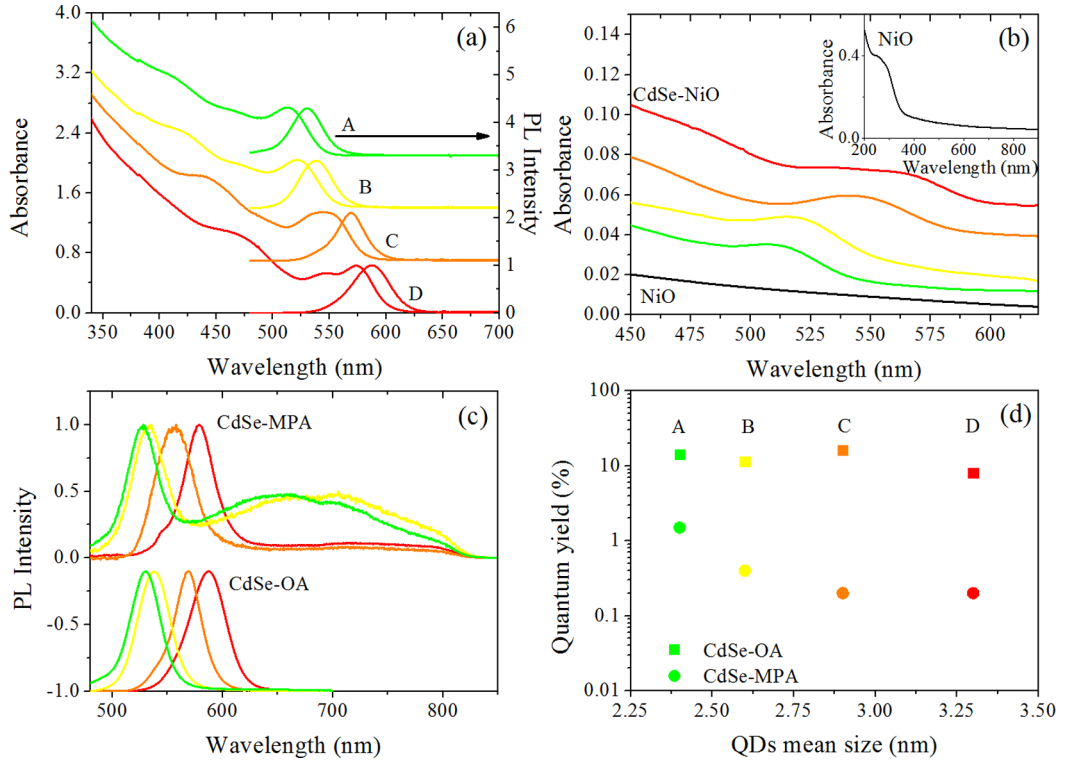

Figure 1. Steady state absorption and PL: (a) absorption and PL spectra of as-obtained oleic acid CdSe QDs in toluene with four different sizes (A, 2.5 nm; B, 2.6 nm; C, 3.0 nm; D, 3.7 nm); (b) absorption spectra of QDs attached onto NiO together with neat NiO (black line) and the inset shows the absorption spectrum of neat NiO with full wavelength scale; (c) PL spectra of QDs with OA capping agent (lower panel) and after linker exchange with MPA capping agent (upper panel); (d) PL quantum yield of MPA-QDs and OA-QDs.

provided. In the final section, we provide an approach to significantly enhance the hole injection efficiency by passivating the surface trapping pathways using core−shell-structured CdSe/ZnS QDs.

EXPERIMENTAL SECTION

Sample Preparation. CdSe QDs for sensitization were synthesized using previously reported methods.[21] The QD size was tuned by controlling the reaction temperature. In this work, reaction temperatures of 230, 240, 260, and 280 °C were used to obtain QDs with diameters of 2.5, 2.6, 3.0, and 3.7 nm, respectively. The synthesis of CdSe/ZnS gradient core−shell quantum dots follows the same procedures as in our previous studies.[19] In brief, Cd^{2+} and Zn^{2+} oleate in 1-octadecene solution was first heated to 325 °C. Then, Se^{2-} and S^{2-} in 3 mL of trioctylphosphine (TOP) solution was swiftly injected into the cation precursor solution. We kept the reaction for 3 min to obtain a shell thickness of 1.3 nm.

In order to attach the QDs to a hole acceptor, the as-obtained capping agent oleic acid was exchanged to the bifunctional linker 3-mercaptopropionic acid (MPA). NiO mesoporous film was prepared according to the method by Sumikura et al.[22] Briefly, the precursor containing $NiCl_2$ and the triblock copolymer F108 dissolved in ethanol was spin-coated onto a glass substrate and then calcined in air at 400 °C for 0.5 h. For further details, see the Supporting Information.

Steady-State Spectroscopy. Ground-state absorption spectra were measured in a UV−vis absorption spectrometer (Agilent 845x). Steady-state photoluminescence was measured using a standard spectrophotometer (Spex 1681) with excitation at 470 nm.

Transient Absorption. Transient absorption spectra were recorded using a pump−probe setup described in our previous study.[21] Briefly, laser pulses (800 nm, 80 fs pulse length, 1 kHz repetition rate) were generated by a regenerative amplifier (Spitfire XP) seeded by a femtosecond oscillator (Tsunami, both Spectra-Physics). Excitation pulses at a wavelength of 450 nm were acquired using an optical parametric amplifier (Topas C, Light Conversion). The used excitation photon flux of 2×10^{14} photons/cm^2/pulse corresponds to $\langle N \rangle \sim 0.2-0.35$ (the mean number of excited e−h pairs per QD, detailed calculation in the Supporting Information), depending on the QD size. The probe pulses (a broad supercontinuum spectrum) were generated from the 800 nm pulses in a sapphire plate and split by a beam splitter into a probe pulse and a reference pulse. The probe pulse and the reference pulse were dispersed in a spectrograph and detected by a diode array (Pascher Instruments). Thin film samples were measured in a nitrogen atmosphere to avoid possible oxidation of QDs.[23]

Time-Resolved Photoluminescence. The laser source for the time-resolved photoluminescence setup is also a titanium:-sapphire passively mode-locked femtosecond laser (Spectra-Physics, Tsunami), emitting at 820 nm with 80 MHz repetition rate and 150 fs pulse length. In order to exclude the possible photocharging process in QDs, we also measured decay kinetics of QDs with different pump repetition rates (80 to 1.6 MHz) keeping the pulse energy unchanged (see the Supporting Information). The laser pulses were frequency-doubled to 410 nm by a second-harmonic generator (Photop technologies, Tripler TP-2000B). The excitation photon flux was 1.1×10^{12} photons/cm^2/pulse corresponding to $\langle N \rangle \sim 0.01-0.05$ depending on the QD size. Time-resolved photoluminescence spectra were detected in a picosecond streak camera (C6860,

dx.doi.org/10.1021/jp506963q | J. Phys. Chem. C 2014, 118, 18462−18471

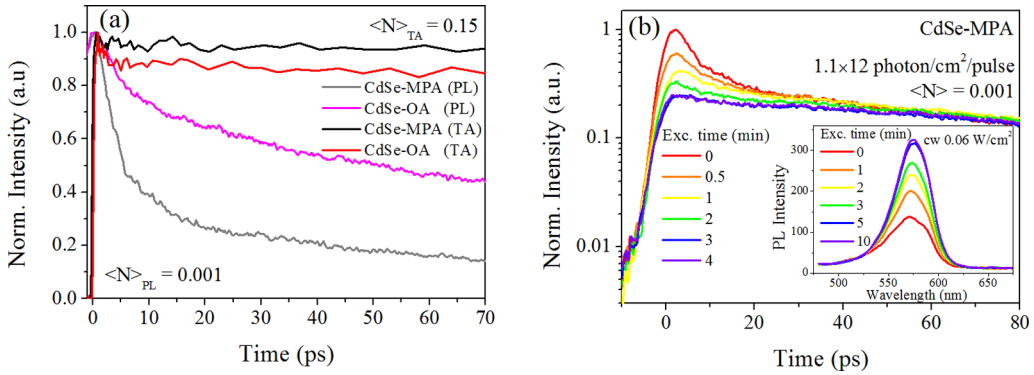

Figure 2. Hole trapping dynamics: (a) TA kinetics at the band-edge absorption and PL decay of CdSe−MPA and CdSe−OA QD film (λ_{exc} = 400 nm, excitation fluence = 1.1 × 10^{12} ph/cm^2/pulse with average photon excitation per QD $\langle N \rangle$ to be 0.001 ph/QD), no photoinduced emission enhancement. (b) Main plot: Evolution of PL decay kinetics of CdSe−MPA after continuous laser irritation. The inset shows the evolution of steady-state PL intensity during the irradiation (λ_{exc} = 448 nm, P_{exc} = 0.06 W/cm^2).

Hamamatsu, time resolution <1 ps) operating in single-shot mode coupled to a Chromex spectrograph, triggered by the Ti:sapphire laser. A long-pass wavelength filter from 490 nm was used in front of the spectrograph to cut off the scattering from the excitation pulses.

RESULTS AND DISCUSSION

Steady-State Spectroscopy. The study was carried out for four CdSe QDs samples with different mean sizes. Figure 1 shows the steady-state absorption and photoluminescence spectra of as-obtained oleic acid-capped QDs in colloidal form. The 1S exciton bands can be well resolved at 512, 520, 548, and 575 nm (defined as QDs A−D, respectively). The mean diameter of QDs can then be calculated to be 2.5, 2.6, 3, and 3.7 nm, respectively.[24] All emission spectra appear at the red side of the absorption edge with a width of ∼25 nm indicating relatively narrow distributions of particle sizes. After deposition on the NiO film, the absorption spectra of the QDs keep the characteristic band-like exciton peaks (Figure 1b) with an offset of the spectra due to light scattering originating from the mesoporous NiO film (inset of Figure 1b). The absorption band edge of a neat NiO film (340 nm) is consistent with the optical band gap of NiO (3.4−4.3 eV).[25]

In order to anchor the QDs onto the NiO acceptor, the long-chained capping agent oleic acid (OA) needs to be replaced by a short-chained linker with bifunctional groups (MPA). However, this linker exchange is known to induce numerous surface defects in the QDs, acting as trapping centers.[26] These trapping centers can originate from different factors, for instance, the unsaturated dangling bonds and attached thiol groups on the surface.[17,26] A direct consequence of this trapping process is the decrease of PL quantum yield (QY), as shown in Figure 1d, where the QYs of QDs after linker exchange to MPA are lower than those of OA-capped QDs (0.2−1.1% vs 9−12%; for the detailed calculation of QY, see the Supporting Information) by more than 1 order of magnitude. In addition, the occurrence of broad defect emission of CdSe−MPA samples with the maximum at wavelengths from 600 to 800 nm in PL spectra (Figure 1c) manifests the possible radiative recombination pathways of trapped charges.[26,27] It should be noted that the contribution of defect emission compared with band-edge emission (2.1−2.4 eV) decreased with the increase of QD sizes, which also accounts for the QY changes in CdSe−MPA QDs with different sizes (Figure 1d).[28] The trend can be explained by the larger surface-to-volume ratio of small QDs, which leads to higher trap concentration.[29]

The presence of an additional emission band and the lower QY indicates that hole trapping plays a significant role in our system. Although carrier trapping has been widely studied before,[16,17] we still need to clarify the trapping dynamics in our system in order to distinguish it from the hole injection.

Hole Trapping Dynamics in CdSe QDs. It has been reported that the hole trapping by thiol molecules can be energetically favorable in thiol-capped CdSe or CdTe quantum dots.[30] This means that injection and trapping processes can happen simultaneously, both leading to charge depopulation and corresponding signal decay. In order to reliably determine the hole injection dynamics, we need to first characterize and understand the trapping process. We study the trapping by comparing the kinetics of PL and TA of the unattached QDs. We point out that the density of the excited electron states at the band-edge transition of CdSe QDs is significantly smaller than the corresponding density of the hole states (in the effective-mass approximation, the lowest excited electron state is only 2-fold degenerate). In addition, the hole states are more closely spaced in QDs.[30,31] As a result, the signal of TA bleaching is dominated by the state filling of electrons instead of holes, whereas the PL measurements are sensitive to both carriers. Consequently, the TA signal provides a means to ascertain or preclude the involvement of electron depopulation in PL quenching.[32]

The difference between the two measurements is very clear in our samples. See, for example, Figure 2a, showing 3.0 nm QDs with the 1S exciton absorption at 548 nm. Here, the TA bleach remains almost the same in OA and MPA-capped QDs within the first 70 ps, whereas a fast decay appears in PL kinetics. Note that the excitation fluence used in both TA ($\langle N \rangle$ = 0.15) and PL ($\langle N \rangle$ = 0.001) measurement is low enough to avoid a significant contribution of multiexciton processes. We can conclude that all PL quenching is related to single-exciton depopulation dominated by hole trapping in this time scale. Furthermore, there is only one exponential decay component with a lifetime of 50 ps in CdSe−OA QDs in the short scanning time window (0−80 ps), while an additional much faster component with a lifetime of 4 ps can be observed in CdSe−MPA QDs. This is a clear hint that a new hole trapping pathway arises after linker exchange.

The lifetime of the fast hole trapping is similar to a value reported in CdTe QDs (1−1.5 ps),[17,27] and the photo-

dx.doi.org/10.1021/jp506963q | J. Phys. Chem. C 2014, 118, 18462−18471

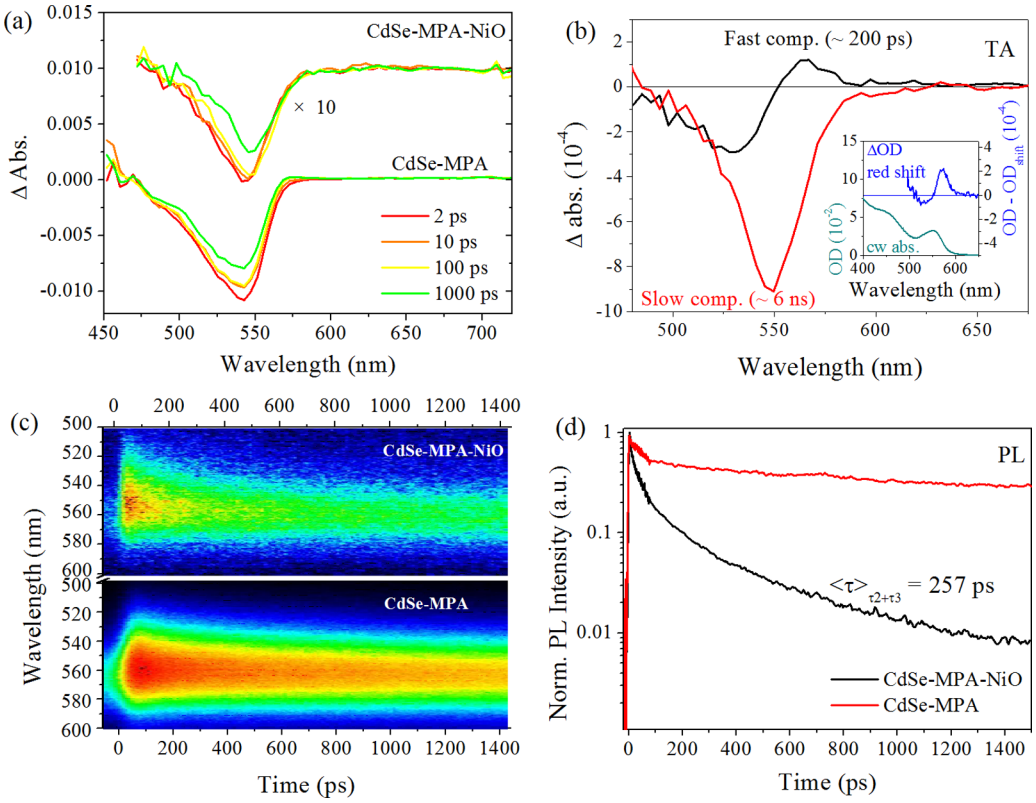

Figure 3. Identifying the hole injection: (a) TA spectra of CdSe−MPA and CdSe−MPA−NiO samples (3.0 nm) under different delay times (2−1000 ps); (b) TA spectral components extracted from the TA data, inset: steady-state absorption spectrum (cyan) and change in absorption after a shift of the spectrum by 10 meV (blue line)—see text for more details; (c) time-resolved PL spectra; (d) PL kinetics of CdSe−MPA and CdSe−MPA−NiO samples with a QD size of 3.0 nm with a time scale up to 1.5 ns. Note that the photoinduced emission enhancement conditions were used (λ_{exc} = 410 nm, $\langle N \rangle$ = 0.001 ph/QD).

generated holes in this case are trapped by the surface dangling bonds induced by the ligand exchange to MPA.[33] This also explains the absence of fast trapping in OA-capped QDs (Figure 1a). We also point out that the multiexponential nature of the hole trapping is the ensemble effect—each kinetic component corresponds to a subselection of the QDs. For example, the photoluminescence of all QDs has the fast trap decay with 4 ps. The origin of the longer components is analogous.

The fast hole trapping, i.e., the 4 ps component, can be gradually diminished by photoirradiation. As shown in Figure 2b, the amplitude of the fast component drastically declines during continuous laser excitation for 4 min, while the longer component becomes somewhat longer. This effect is well-known as photoinduced emission enhancement (PEE) which leads to an increase in photoluminescence intensity with continuous photoirradiation, as also shown in the inset of Figure 1b.[34−36] The effect is commonly explained by surface passivation induced by the chemical changes of the QD surface during photoirradiation[37,38] and photoactivation which switches dark quenched dots to bright fluorescing dots.[34,36] While the contribution of the fast hole trapping to the kinetics can be diminished by the PEE, the slow hole trapping is not sensitive to the irradiation. These observations are consistent with previously reported hole trapping rates.[29,39]

Identification of Hole Injection in the CdSe−NiO System. Equipped by the detailed account of the hole trapping dynamics in the case of pure QDs, we turn now to the case when CdSe QDs are attached to NiO and thereby hole injection can occur. A complementary analysis combining TA and time-resolved PL was performed. As mentioned above, the TA bleaching dynamics is not sensitive to closely spaced hole states; thus, the bleach kinetics in the visible to near-IR wavelength region does not directly reflect the state filling of hole species. However, changes in the energy levels in QDs contribute to the TA signal. In particular, after hole injection, the QDs are negatively charged and the absorption of such negatively charged QDs can differ from the absorption of neutral excited QDs. TA measurement can thereby still provide detectable changes in some spectral regions.

Figure 3a shows typical TA spectra with different delay times, from 2 to 1000 ps, on two different samples: MPA-capped CdSe QDs deposited onto a glass substrate or attached to NiO. The amplitude of the TA signal of the CdSe−NiO sample was magnified by a factor of 10 for clear comparison. Generally, the two samples show similar bleach spectra due to the electron population of the 1S state after excitation. Nevertheless, the bleach band of CdSe−MPA−NiO exhibits a narrower width and larger asymmetry at the red side compared with that of CdSe−MPA. We carried out a global fitting of the measured kinetics for all probe wavelengths. Two components can be obtained from the fitting. One component shows bleach with the minimum at the band-edge absorption (548 nm) with long lifetime (6 ± 2 ns), which is dominating the TA evolution. This component reflects the long-lived signal originating from electron state filling. The second component is rising with a time constant of about 200 ps and shows negative bleach at 530 nm and positive absorption at 570 nm. The spectral shape

dx.doi.org/10.1021/jp506963q | J. Phys. Chem. C 2014, 118, 18462−18471

of the component resembles the first derivative of the absorption spectrum (see the cyan line in the inset of Figure 3b), which is a typical manifestation of the energy level shift.[30]

We can explain this component by employing a charged-QD absorption model (inset of Figure 3b). If negatively charged, the absorption edge of the QDs would show a red shift. The red shift connected to an extra electron in the QDs is typically on the scale of a few meV, as was reported before in the literature.[40,41]

We use the linear absorption spectrum of the QDs to simulate the TA signal from the charged QDs. We assume that charging leads to a 10 meV red-shifted spectrum. By calculating the difference between the shifted (negatively charged) and the original (uncharged, cyan line in the inset of Figure 3b) spectra, we obtain a curve (blue line in Figure 3b inset) with amplitude and shape very similar to the 200 ps component of the TA spectrum (black line in Figure 3b). The observed shift in the TA decay should not be confused by the biexcitonic shift. The biexcitonic shift is present in all our samples (both films and solutions) immediately after excitation and leads to excited-state-absorption features at short delays below 1 ps (see the Supporting Information for details). The feature is rapidly covered by the dominating bleach signal. The biexcitonic shift decays together with the bleach, and it is, therefore, included in the 6 ns component.

It should be noted that the charged QDs are unlikely to be formed directly by laser excitation due to low excitation fluence (0.15 ph/QDs) and low photon energy (exc. wavelength of 450 nm), which is well below the weak photoionization threshold identified for QDs.[42] In the time-resolved PL studies below, we have also carried out control experiments where the pump repetition rate was changed, leaving the pulse energy the same. No changes in the PL kinetics were seen, providing evidence of negligible direct photocharging of the QDs.

The observed shift in the TA spectra is a piece of indirect evidence but not the full proof of hole injection into NiO. However, we point out that it is clear that the TA evolution of the QD−MPA sample (no spectral shift of the TA signal) is quite different from the case of QD−MPA−NiO (a clear red shift of the TA spectra at long delays). If we take into account that hole trapping is very efficient for the QD−MPA samples (see Figure 2a), the TA behavior for the QD−MPA−NiO case cannot be explained by a simple hole trapping on the QD surface. Thus, we assign the appearance of the negatively charged QDs to the hole injection into NiO.

PL decay is a more direct way of investigating hole injection. PL spectrograms of CdSe−NiO and CdSe QDs deposited on glass are shown in Figure 3c. Clearly, quenching in the system with NiO is significantly faster. In addition, spectral asymmetry can be found in both samples with faster decay at shorter wavelengths. This originates from variations in the hole trapping for different-size QDs and partially also manifests Förster energy transfer within QD clusters.[43−45] Because all QDs are directly attached to the NiO, we can average the PL kinetics over the whole detection region (500−600 nm) so that the distortions due to the possible intra-QD Förster transfer within clusters of QDs would be canceled out (for each decay of the excitation donor fluorescence, there is a corresponding rise of the acceptor fluorescence; see the Supporting Information for further justification). What remains is the kinetics corresponding to the internal dynamics of the QDs and injection into the NiO. The kinetics in Figure 3d (QD size of 3.0 nm) can be fitted biexponentially with time constants τ_1 = 52 ps (46%) and τ_2 = 3.0 ns (54%) for neat CdSe and triexponentially with time constants τ_1 = 4.1 ps (35%), τ_2 = 43 ps (54%), and τ_3 = 377 ps (11%) for CdSe−NiO. Analogous results can be obtained for all QD sizes (see Table 1). The common ∼50 ps component remains almost unchanged by QD sensitization and is attributed to quenching by slow defect trapping. As mentioned above, in the neat QDs, the surface trapping would gradually be diminished during photoirradiation (known as the PEE process). However, the surface-trapping-related fast component (4.1 ps) in CdSe−NiO remains unchanged even after long-time irradiation. This has two possible explanations: (1) Attachment to NiO may prevent PEE, since photo-oxidation can be hindered because oxygen molecules cannot easily penetrate into the CdSe−NiO interface. (2) Charging of the QDs by hole injection leads to efficient photodegradation which can surpass the PEE effect.[23,46] The slow component (380 ps) in the CdSe−NiO system is very different from the excited-state lifetime in the neat CdSe QDs and is comparable to the 200 ps component derived from TA, taking into account the experimental error of the TA fitting (about 100 ps). This means that an extra hole depopulation pathway is induced by the NiO attachment, which can be observed in the TA measurement as a QD charging process. We therefore gain more support for the assignment of the component to hole injection from QD to NiO.

Table 1. Multi-Exponential Fitting Parameters

sample	A_1	τ_1 (ps)	A_2	τ_2 (ps)	A_3	τ_3 (ps)
512MPA (2.5 nm)			0.51	45	0.49	3529
512NiO	0.76	3.2	0.19	40	0.05	1537
520MPA (2.6 nm)			0.49	43	0.51	2819
520NiO	0.39	5.3	0.52	66	0.09	785
548MPA (3.0 nm)			0.49	56	0.51	2852
548NiO	0.71	4.8	0.24	52	0.05	344
575MPA (3.7 nm)			0.36	122	0.64	2696
575NiO	0.54	5.2	0.30	49	0.15	300

The assignment can be further supported by several considerations. First, the dynamics on the time scale of hundreds of picoseconds can be observed in both TA (QD charging) and PL decay. In contrast, the hole trapping does not lead to a corresponding decay in the TA signal. Second, the injection component amplitude in PL emission (∼10%) is close to the incident-current-to-photon conversion efficiency (IPCE) of CdSe QD−NiO photoanodes in real device applications reported elsewhere.[11] As the hole trapping process is significantly faster in our QDs compared to the hole injection, all the QDs suffering from even a single trapping site will feature a low hole injection efficiency. The injection component can therefore only be observed if QDs are well passivated.

QD Size Dependence of Hole Injection in the CdSe−NiO System. Numerous studies of electron injection in QD−MO systems revealed that the transfer rate k_{ET} is influenced by the free energy change (also known as the driving force) ΔG which can be tuned by QD size.[20,21] We expect the same tendency for hole injection in our CdSe−NiO system. The hole injection kinetics of QDs with different sizes (2.5−3.7 nm) are illustrated in Figure 4. An additional quenching component can be found in all CdSe−NiO samples (Figure 4b) compared with neat CdSe QDs (Figure 4a), and its lifetime varies with QD size.

dx.doi.org/10.1021/jp506963q | J. Phys. Chem. C 2014, 118, 18462−18471

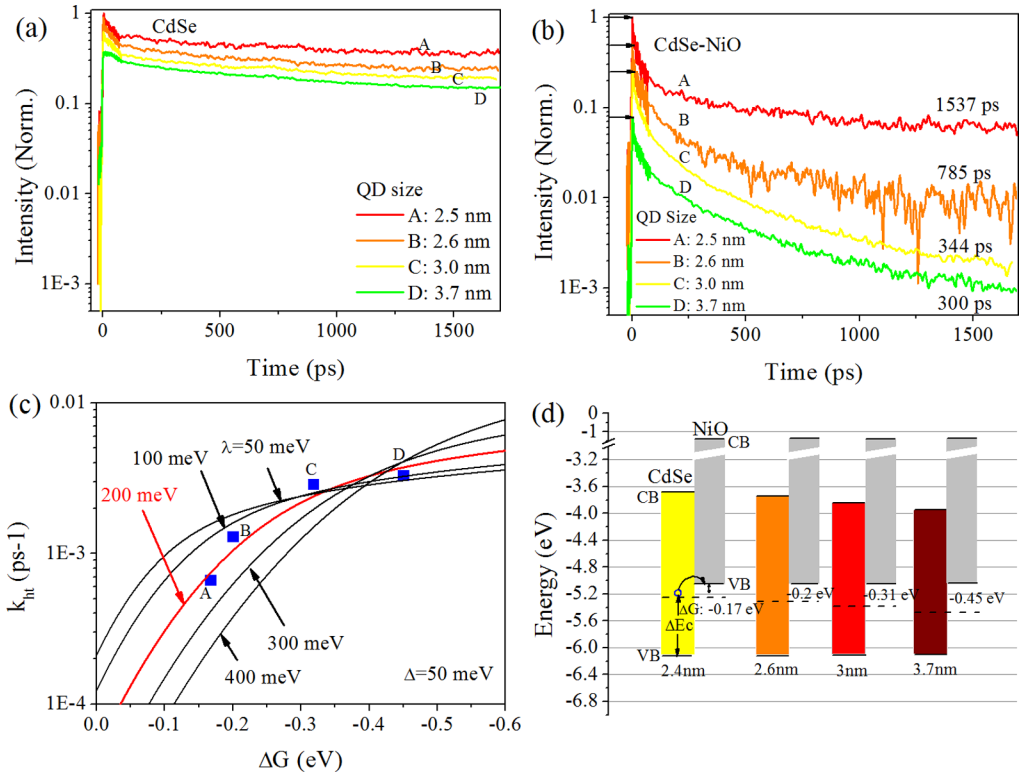

Figure 4. Hole injection rate as a function of driving force: (a) PL kinetics of CdSe−MPA and (b) CdSe−MPA−NiO samples with four different QD sizes; (c) hole injection rate vs driving force of different sizes of QDs (A, 2.5 nm; B, 2.6 nm; C, 3.0 nm; D, 3.7 nm) attached to NiO (blue squares) and fitting curves (black and red lines); (d) corresponding energy alignment of the CdSe−NiO system.

On the basis of the detailed multiexponential fitting analyses (see Table 1), we found that the time constants of trapping-related processes (τ_1 and τ_2) show only minor changes with QD size. However, the lifetime of the injection component increases with decreasing QD size. According to previous studies of QD electron injection, the driving force ΔG consists of the electron energy difference ΔE_{el} (different conduction band bottom between CdSe and MO) and the Coulomb interaction ΔE_c between injected electrons in the acceptor and holes in QDs which acts against the electron transfer.[20] Both are affected by QD sizes. We can trace the driving force of hole injection using the same strategy:

$$\Delta G = \Delta E_{hl} + \Delta E_c \quad (1)$$

where ΔE_{hl} stands for the hole energy difference. According to a previous report employing XPS measurements, the position of the highest "valence band" levels of CdSe QDs (VBM_{CdSe}) is independent of QD size when attached to MO.[18] VBM_{CdSe} is around −6.09 eV with respect to a vacuum, while the VBM of NiO (VBM_{NiO}) was reported to be +0.54 eV vs NHE (−5.04 eV vs vacuum) in the similar CdSe QD−NiO system.[47] Thus, we can determine the hole energy difference $\Delta E_{hl} = VBM_{CdSe} - VBM_{NiO} = -1.05$ eV, which is QD-size-independent. The expression to calculate ΔE_c in QD−MO systems has been reported elsewhere:[20]

$$\Delta E_C = \frac{1.786e^2}{\varepsilon_{QD}R_{QD}} + \frac{e^2}{2R_{QD}}\left(1 + \frac{0.786}{\varepsilon_{QD}}\right) - \frac{e^2}{4(R_{QD}+h)}\frac{\varepsilon_{MO}-1}{\varepsilon_{MO}+1} \quad (2)$$

where $\varepsilon_{QD} = 6.1$[20] and $\varepsilon_{NiO} = 12$[48] are the permittivity of QDs and NiO, repectively. R_{QD} is the mean radius of the QDs, which varies from 1.25 to 1.85 nm in our case. $h = 0.65$ nm is the QD−MO distance, which is also the linker layer thickness of 3-MPA. ΔE_c is found to be 0.83, 0.80, 0.69, and 0.55 eV for QDs with sizes of 2.5, 2.6, 3.0, and 3.7 nm, respectively. As summarized in Table 2, although the valence band maximum remains almost unchanged with QD size, resulting in a fixed E_{hl}, the total driving force still shows a big difference from −0.17 to −0.45 eV due to the size-dependent Coulomb energy.

Table 2. Calculation of the Driving Force for Hole Injection

QD size (nm)	ΔE_{hl}[a] (eV)	ΔE_c[b] (eV)	ΔG[c] (eV)	k_{ht}[d] (ps^{-1})
2.5	−1.0	0.83	−0.17	6.7×10^{-4}
2.6	−1.0	0.80	−0.20	0.0013
3.0	−1.0	0.69	−0.31	0.0029
3.7	−1.0	0.55	−0.45	0.0033

[a]The hole energy difference between QDs and NiO. [b]Columbic interaction energy between injected holes in NiO and electrons in QDs. [c]Calculated driving force. [d]Hole injection rates.

We analyze the hole injection rates $k_{ht} = 1/\tau_3$ (see Table 1) as a function of the driving force ΔG by means of the Marcus theory of charge transfer, which is widely used in electron injection studies of QD−MO systems:

$$k_{ET} = C\int_{-\infty}^{\infty}\rho(E)\exp\left(-\frac{(\lambda + \Delta G + E)^2}{4\lambda k_B T}\right)dE \quad (3)$$

where k_{ET}, k_B, and λ are the electron transfer rate, Boltzmann's constant, and system reorganizational energy, respectively. C is the scaling factor including all energy-independent coefficients

dx.doi.org/10.1021/jp506963q | J. Phys. Chem. C 2014, 118, 18462−18471

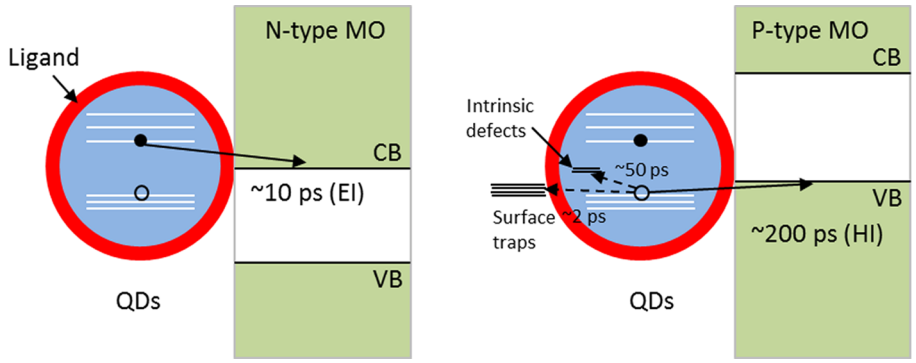

Figure 5. Schematics of electron injection (left) and hole injection (right) processes when QDs are attached to n-type electron acceptors and p-type hole acceptors; the time scale of electron injection is derived from our previous results.[17]

(i.e., Marcus theory prefactors and the wave function overlap). $\rho(E)$ represents the density of unoccupied states in the MO acceptor. Here, we can directly transform the expression of election injection rate to hole injection rate k_{ht}:

$$k_{ht} = C\int_{-\infty}^{\infty}\rho(E)\exp\left(-\frac{(\lambda+\Delta G+E)^2}{4\lambda k_B T}\right)\mathrm{d}E \quad (4)$$

In nanostructured MO, the density of states can be described by a theory introduced by Katoh et al. as a convolution between bulk-like DOS ρ_0 with Gaussian-distributed band-edge states featuring the dispersion Δ:[49,50]

$$\rho(E) = \int_0^{\infty}\rho_0(E')V_0\frac{1}{\Delta\sqrt{2\pi}}\mathrm{e}^{-(E-E')^2/2\Delta^2}\,\mathrm{d}E' \quad (5)$$

Here, V_0 represents the volume of the crystal and Δ characterizes the density of band-edge states induced by the surface disorder, different doping levels within the nanostructure, and other sources of disorder. Values of Δ vary according to the materials and morphology of the structure. In our previous work, we presented a practical way to evaluate Δ according to the band-edge absorption Urbach tail in the absorption spectra.[49] Due to the strong scattering of the NiO film, it is difficult to use the same method here. Thus, we selected the typical value of 50 meV in QD−MO nanoparticle systems during the fitting.[20] In addition, the effect of variation of Δ on the fitting also shows that 50 meV is a reasonable estimation for our system (see the Supporting Information).

The red line in Figure 4c gives the best fit to our data by using a reorganization energy of 200 meV. By fixing the reorganizational energy to other values, we were not able to reproduce the obtained ΔG dependence (see black lines and the Supporting Information for details). Theoretically, the reorganization energy is related to the donor−acceptor interface condition (e.g., ligand molecules on the QD surface) as well as the system surroundings (e.g., a solvent or buffer layer in the system). Generally speaking, the reorganization energy varies in a wide range with different interface and surroundings conditions. Here, we found a relatively high reorganization energy of 190 meV in our CdSe−ZnO samples which is analogous to our previous reports.[51]

In Figure 4d, we have depicted the driving force of the hole injection in the case of the different QD sizes used in the current study. The figure illustrates the possibility for energy engineering in p-type QD solar cells or QD photocathodes by QD size.

We are using the nonadiabatic Marcus theory to describe the hole injection in our QD−linker−MO system. In this context, the recent calculations of the QD−TiO_2 system deserve a comment.[52] In this study, thorough nonadiabatic molecular dynamics simulations of the photoinduced electron injection from QDs to TiO_2 were performed. The authors conclude that the electron transfer proceeds via the adiabatic mechanism where optical phonons play an important role. We point out that, in the system which was calculated, the QD was in direct contact with the MO, leading to strong interaction. In our case, QDs are covered by a layer of linker molecules which provide the attachment to the MO. This reduces the interaction significantly which changes the electron transfer regime. It would be interesting to study the electron and hole injection from such directly attached QDs which can be prepared via the so-called SILAR technique.[53]

Comparing the hole injection in our CdSe−NiO system with the electron injection in the n-type CdSe−ZnO system in our previous studies,[21,54] we see that the hole injection is more than an order of magnitude slower than the electron injection, as shown in Figure 5. This can be attributed to different factors: (1) the larger effective mass of holes ($m_{hCdSe}/m_{eCdSe} > 3$) and (2) the low permittivity of p-type materials (i.e., NiO) compared with n-type electron acceptors (i.e., ZnO, TiO_2), which leads to large localized electron−hole Coulomb interaction inhibiting the charge transfer as discussed above. However, the most critical factor restricting the hole injection efficiency is the hole trapping which is competing with injection. According to our results, only about 5−15% of holes are transferred to NiO, while most of them are trapped either by the ligand group or lattice defects. This is consistent with results of p-type solar cell performance where an external quantum efficiency below 10% was observed using CdSe QD-sensitized NiO as photoanodes.[9] Therefore, in order to enhance the hole transfer efficiency, passivation of the hole traps (i.e., using core−shell structures) is essential.

Hole Injection from Surface Passivated Core−Shell QDs. As mentioned, surface trapping is the dominating process competing with hole injection. Only 5−15% of the QDs free from the surface traps can inject holes into NiO. Thus, we can expect a great improvement of the hole injection efficiency by passivation of such traps. To achieve that, we have made CdSe/ZnS gradient core−shell QDs and attached them to NiO. Such QDs have a high degree of surface passivation confirmed by a high emissive quantum yield. On the other hand, the gradually changed band edge from core to shell ensures sufficient

dx.doi.org/10.1021/jp506963q | J. Phys. Chem. C 2014, 118, 18462−18471

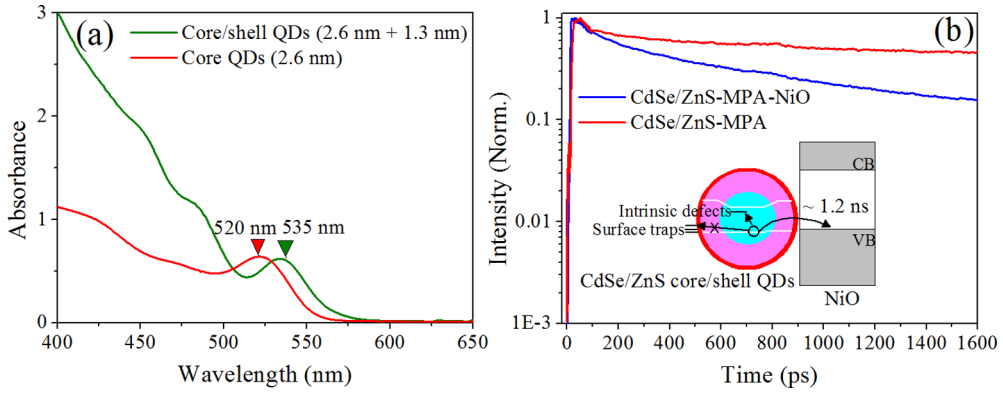

Figure 6. (a) Absorption spectra of neat CdSe QDs (green) and CdSe/ZnS core−shell QDs (red) in colloidal form. (b) PL kinetics of CdSe/ZnS core−shell QDs (4 nm mean size) with MPA capping and the core−shell QD−MPA−NiO sample (λ_{exc} = 410 nm). The inset illustrates the band alignment for hole injection between core−shell QDs and NiO.

electronic coupling between QDs and metal oxide acceptors even with the large spacing caused by the shell.[19]

Here, we employed core−shell QDs with 2.6 nm core size and 1.3 nm shell thickness, which has been proven to be the optimal condition for electron injection when attached to ZnO. Compared with conventional pristine QDs with the same core size (2.6 nm), the 1S exciton band of core−shell QDs exhibits a red shift (~15 nm) in the absorption spectrum, as shown in Figure 6a, indicating enlarged effective size due to the shell. Analogous PL kinetics measurements as above were carried out with the core−shell QDs (see Figure 6b). Due to good surface passivation, the fast trapping component (within a time scale of tens of picoseconds) totally disappears in both neat core−shell QD−MPA and core−shell QD−MPA−NiO samples. The medium-fast component, which we assigned to defect trapping within the QD volume, still remains. Apart from that, in QD−NiO samples, we can observe an additional component of 1−2 ns which is absent in the QD-only sample. The component is clearly the hole injection. The injection time is determined via the three-exponential fitting procedure to be around 1.2 ns (see Table 3). This value is slower than pristine core QDs with the same core size (2.6 nm) owing to the increased spacing due to the shell. However, the decrease of the transfer rate is not as large as one would expect merely on the basis of the tunneling distance argument. This is probably because the core electronic states can penetrate into the shell because of the gradient character of the shell. This can enhance the donor−acceptor electronic coupling, which can be further increased by the fact that valence band alignment in the CdSe materials is very "flat".[19,55]

Table 3. Multi-Exponential Fitting Parameters for Core−Shell Quantum Dots

sample	A_1	τ_1 (ps)	A_2	τ_2 (ps)	A_3	τ_3 (ps)
core−shell QDs−MPA			0.61	43	0.39	3962
core−shell QDs−NiO			0.56	117	0.53	1227
core QDs−NiO	0.39	5.3	0.52	66	0.09	785

An important improvement in the case of core−shell QDs is that the efficiency of the hole injection rises from less than 10 to 50%. This is a clear enhancement of the hole collection efficiency, achieved by passivation of surface trapping.

CONCLUSION

We have investigated the photodynamics of holes in CdSe QDs via complementary TA and time-resolved PL spectroscopies. Two different classes of hole trapping sites were resolved in QDs with lifetimes of several picoseconds and tens of picoseconds, respectively. The surface hole traps with a trapping time of several picoseconds can be passivated by photoinduced surface chemical change, exhibiting a gradual decrease of the faster quenching pathway of PL.

After attaching QDs to the hole acceptor NiO, the dynamics of hole injection can be observed with a time scale of several hundred picoseconds, much slower than the electron injection in a similar system. We further demonstrate that the injection rates can be tuned by QD size via changing of the driving force ΔG. In addition, we demonstrated that, by passivation of surface traps, the hole injection efficiency is enhanced by more than 5 times. These results reveal details of the hole transfer in the photocathode of p-type QD solar cells and demonstrate an immense potential of using suitable core−shell structures in p-type solar cells.

ASSOCIATED CONTENT

Supporting Information

Details of sample preparation; emission quantum yield and average excitation fluence calculation; fitting of PL kinetics; and effect of spectral diffusion and pump pulse repetition rate on PL kinetics. This material is available free of charge via the Internet at http://pubs.acs.org.

AUTHOR INFORMATION

Corresponding Authors

*E-mail: Kaibo.Zheng@chemphys.lu.se.
*E-mail: Tonu.Pullerits@chemphys.lu.se.

Author Contributions

Kaibo Zheng, Karel Žídek, and Mohamed Abdellah contributed equally to this work.

Notes

The authors declare no competing financial interest.

ACKNOWLEDGMENTS

The study was financially supported by the Swedish Energy Agency, the Knut and Alice Wallenberg Foundation, and the Swedish Research Council. Collaboration within nmC@LU is acknowledged.

REFERENCES

(1) Sambur, J. B.; Novet, T.; Parkinson, B. A. Multiple Exciton Collection in a Sensitized Photovoltaic System. *Science* **2010**, *330*, 63−66.

(2) Kamat, P. V. Quantum Dot Solar Cells. The Next Big Thing in Photovoltaics. *J. Phys. Chem. Lett.* **2013**, *4*, 908−918.

(3) Nozik, A. J.; Beard, M. C.; Luther, J. M.; Law, M.; Ellingson, R. J.; Johnson, J. C. Semiconductor Quantum Dots and Quantum Dot Arrays and Applications of Multiple Exciton Generation to Third-generation Photovoltaic Solar Cells. *Chem. Rev.* **2010**, *110*, 6873−6890.

(4) Ellingson, R. J.; Beard, M. C.; Johnson, J. C.; Yu, P.; Micic, O. I.; Nozik, A. J.; Shabaev, A.; Efros, A. L. Highly Efficient Multiple Exciton Generation in Colloidal PbSe and PbS Quantum Dots. *Nano Lett.* **2005**, *5*, 865−871.

(5) Ip, A. H.; Thon, S. M.; Hoogland, S.; Voznyy, O.; Zhitomirsky, D.; Debnath, R.; Levina, L.; Rollny, L. R.; Carey, G. H.; Fischer, A.; Kemp, K. W.; Kramer, I. J.; Ning, Z.; Labelle, A. J.; Chou, K. W.; Amassian, A.; Sargent, E. H. Hybrid Passivated Colloidal Quantum Dot Solids. *Nat. Nanotechnol.* **2012**, *7*, 577−582.

(6) Karki, K. J.; Ma, F.; Zheng, K.; Žídek, K.; Mousa, A.; Abdellah, M.; Messing, M. E.; Wallenberg, L. R.; Yartsev, A.; Pullerits, T. Multiple Exciton Generation in Nano-crystals Revisited: Consistent Calculation of the Yield Based on Pump-probe Spectroscopy. *Sci. Rep.* **2013**, *3*, 2287.

(7) Žídek, K.; Zheng, K.; Abdellah, M.; Lenngren, N.; Chábera, P.; Pullerits, T. Ultrafast Dynamics of Multiple Exciton Harvesting in the CdSe−ZnO System: Electron Injection versus Auger Recombination. *Nano Lett.* **2012**, *12*, 6393−6399.

(8) Santra, P. K.; Kamat, P. V. Mn-doped Quantum Dot Sensitized Solar Cells: A Strategy to Boost Efficiency over 5%. *J. Am. Chem. Soc.* **2012**, *134*, 2508−2511.

(9) Leschkies, K. S.; Divakar, R.; Basu, J.; Enache-Pommer, E.; Boercker, J. E.; Carter, C. B.; Kortshagen, U. R.; Norris, D. J.; Aydil, E. S. Photosensitization of ZnO Nanowires with CdSe Quantum Dots for Photovoltaic Devices. *Nano Lett.* **2007**, *7*, 1793−1798.

(10) Jovanovski, V.; González-Pedro, V.; Giménez, S.; Azaceta, E.; Cabañero, G.; Grande, H.; Tena-Zaera, R.; Mora-Seró, I.; Bisquert, J. A Sulfide/polysulfide-based Ionic Liquid Electrolyte for Quantum Dot-sensitized Solar Cells. *J. Am. Chem. Soc.* **2011**, *133*, 20156−20159.

(11) Barceló, I.; Guillén, E.; Lana-Villarreal, T.; Gómez, R. Preparation and Characterization of Nickel Oxide Photocathodes Sensitized with Colloidal Cadmium Selenide Quantum Dots. *J. Phys. Chem. C* **2013**, *117*, 22509−22517.

(12) Wang, Z.; Shakya, A.; Gu, J.; Lian, S.; Maldonado, S. Sensitization of p-GaP with CdSe Quantum Dots: Light-Stimulated Hole Injection. *J. Am. Chem. Soc.* **2013**, *135*, 9275−9278.

(13) Vos, A. D. Detailed balance limit of the efficiency of tandem solar cells. *J. Phys. D* **1980**, *13*, 839.

(14) Mori, S.; Fukuda, S.; Sumikura, S.; Takeda, Y.; Tamaki, Y.; Suzuki, E.; Abe, T. Coumarin 343−NiO Films as Nanostructured Photocathodes in Dye-Sensitized Solar Cells: Ultrafast Electron Transfer, Effect of the I^{3-}/I^{-} Redox Couple and Mechanism of Photocurrent Generation. *J. Phys. Chem. C* **2008**, *112*, 16134−16139.

(15) Li, L.; Gibson, E. A.; Qin, P.; Boschloo, G.; Gorlov, M.; Hagfeldt, A.; Sun, L. Double-Layered NiO Photocathodes for p-Type DSSCs with Record IPCE. *Adv. Mater.* **2010**, *22*, 1759−1762.

(16) Jones, M.; Lo, S. S.; Scholes, G. D. Quantitative Modeling of the Role of Surface Traps in CdSe/CdS/ZnS Nanocrystal Photoluminescence Decay Dynamics. *Proc. Natl. Acad. Sci. U.S.A.* **2009**, *106*, 3011−3016.

(17) Kaniyankandy, S.; Rawalekar, S.; Verma, S.; Palit, D. K.; Ghosh, H. N. Charge Carrier Dynamics in Thiol Capped CdTe Quantum Dots. *Phys. Chem. Chem. Phys.* **2010**, *12*, 4210−4216.

(18) Carlson, B.; Leschkies, K.; Aydil, E. S.; Zhu, X. Y. Valence Band Alignment at Cadmium Selenide Quantum Dot and Zinc Oxide $(10\bar{1}0)$ Interfaces. *J. Phys. Chem. C* **2008**, *112*, 8419−8423.

(19) Abdellah, M.; Žídek, K.; Zheng, K.; Chábera, P.; Messing, M. E.; Pullerits, T. Balancing Electron Transfer and Surface Passivation in Gradient CdSe/ZnS Core−Shell Quantum Dots Attached to ZnO. *J. Phys. Chem. Lett.* **2013**, *4*, 1760−1765.

(20) Tvrdy, K.; Frantsuzov, P. A.; Kamat, P. V. Photoinduced Electron Transfer from Semiconductor Quantum Dots to Metal Oxide Nanoparticles. *Proc. Natl. Acad. Sci. U.S.A.* **2011**, *108*, 29−34.

(21) Žídek, K.; Zheng, K.; Ponseca, C. S.; Messing, M. E.; Wallenberg, L. R.; Chábera, P.; Abdellah, M.; Sundström, V.; Pullerits, T.; Žídek, K. Electron Transfer in Quantum-dot-sensitized ZnO Nanowires: Ultrafast Time-resolved Absorption and Terahertz Study. *J. Am. Chem. Soc.* **2012**, *134*, 12110−12117.

(22) Sumikura, S.; Mori, S.; Shimizu, S.; Usami, H.; Suzuki, E. Syntheses of NiO Nanoporous Films Using Nonionic Triblock Copolymer Templates and their Application to Photo-cathodes of p-type Dye-sensitized Solar Cells. *J. Photochem. Photobiol., A* **2008**, *199*, 1−7.

(23) Žídek, K.; Zheng, K.; Chábera, P.; Abdellah, M.; Pullerits, T. Quantum Dot Photodegradation due to CdSe-ZnO Charge Transfer: Transient Absorption Study. *Appl. Phys. Lett.* **2012**, *100*, 243111.

(24) Yu, W.; Qu, L.; Guo, W.; Peng, X. Experimental Determination of the Extinction Coefficient of CdTe, CdSe, and CdS Nanocrystals. *Chem. Mater.* **2003**, *15*, 2854−2860.

(25) Irwin, M. D.; Buchholz, D. B.; Hains, A. W.; Chang, R. P. H.; Marks, T. J. P-Type Semiconducting Nickel Oxide as an Efficiency-enhancing Anode Interfacial Layer in Polymer Bulk-heterojunction Solar Cells. *Proc. Natl. Acad. Sci. U.S.A.* **2008**, *105*, 2783−2787.

(26) Omogo, B.; Aldana, J. F.; Heyes, C. D. Radiative and Nonradiative Lifetime Engineering of Quantum Dots in Multiple Solvents by Surface Atom Stoichiometry and Ligands. *J. Phys. Chem. C* **2013**, *117*, 2317−2327.

(27) Klimov, V. I.; McBrach, D. W. Electron and Hole Relaxation Pathways in Semiconductor Quantum Dots. *Phys. Rev. B* **1999**, *60*, 13740−13749.

(28) Kim, S. M.; Yang, H. S. Radiative Decay of Surface-trapped Carriers and Quantum Yield in CdSe Nanocrystal Quantum Dots. *Curr. Appl. Phys.* **2011**, *11*, 1056−1059.

(29) Babentsov, V.; Sizov, F. Defects in Quantum Dots of IIB−VI Semiconductors. *Opto-Electron. Rev.* **2008**, *16*, 208−225.

(30) Klimov, V. I. Spectral and Dynamical Properties of Multi-excitons in Semiconductor Nanocrystals. *Annu. Rev. Phys. Chem.* **2007**, *58*, 635−673.

(31) Malko, A. V.; Mikhailovsky, A. A.; Petruska, M. A.; Hollingsworth, J. A.; Klimov, V. I. Interplay between Optical Gain and Photoinduced Absorption in CdSe Nanocrystals. *J. Phys. Chem. B* **2004**, *108*, 5250−5255.

(32) Rowland, C. E.; Shaller, R. D. Exciton Fate in Semiconductor Nanocrystals at Elevated Temperatures: Hole Trapping Outcompetes Exciton Deactivation. *J. Phys. Chem. C* **2013**, *117*, 17337−17343.

(33) Wuister, S. F.; Donegá, C. M.; Meijerink, A. Influence of Thiol Capping on the Exciton Luminescence and Decay Kinetics of CdTe and CdSe Quantum Dots. *J. Phys. Chem. B* **2004**, *108*, 17393−17397.

(34) Jones, M.; Nedeljkovic, J.; Ellingson, R. J.; Nozik, A. J.; Rumbles, G. Photoenhancement of Luminescence in Colloidal CdSe Quantum Dot Solutions. *J. Phys. Chem. B* **2003**, *107*, 11346−11352.

(35) Javier, A.; Strouse, G. F. Activated and Intermittent Photoluminescence in Thin CdSe Quantum Dot Films. *Chem. Phys. Lett.* **2004**, *391*, 60−63.

(36) Christova, C. G.; Stouwdam, J. W.; Eijkemans, T. J.; Silov, A. Y.; Van der Heijden, R. W.; Kemerink, M.; Janssen, R. A. J.; Salemink, H. W. M. Photoluminescence Enhancement in Thin Films of PbSe Nanocrystals. *Appl. Phys. Lett.* **2008**, *93*, 121906.

(37) Nazzal, A. Y.; Qu, L.; Peng, X.; Xiao, M. Photoactivated CdSe Nanocrystals as Nanosensors for Gases. *Nano Lett.* **2003**, *2*, 819−822.

(38) Peterson, J. J.; Krauss, T. D. Photobrightening and Photodarkening in PbS Quantum Dots. *Phys. Chem. Chem. Phys.* **2006**, *8*, 3851−3856.

(39) Gómez-Campos, F. M.; Califano, M. Hole Surface Trapping in CdSe Nanocrystals: Dynamics, Rate Fluctuations, and Implications for Blinking. *Nano Lett.* **2012**, *12*, 4508−4517.

(40) Stinaff, E. A.; Schelbner, M.; Bracker, A. S.; Ponomarev, I. V.; Korenev, V. L.; Ware, M. E.; Doty, M. F.; Reinecke, T. L.; Gammon,

D. Optical Signatures of Coupled Quantum Dots. *Science* **2006**, *311*, 636−639.
(41) Hartmann, A.; Ducommun, Y.; Kapon, E.; Hohenester, U.; Molinari, E. Few-particle Effects in Semiconductor Quantum Dots: Observation of Multicharged Excitons. *Phys. Rev. Lett.* **2000**, *84*, 5648−5651.
(42) Saba, M.; Aresti, M.; Quochi, F.; Marceddu, M.; Loi, M. A.; Huang, J.; Talapin, D. V.; Mura, A.; Bongiovanni, G. Light-induced Charged and Trap States in Colloidal Nanocrystals Eetected by Variable Pulse Rate Photoluminescence Spectroscopy. *ACS Nano* **2013**, *7*, 229−238.
(43) Zheng, K.; Žídek, K.; Abdellah, M.; Torbjörnsson, M.; Chábera, P.; Shao, S.; Zhang, F.; Pullerits, T. Fast Monolayer Adsorption and Slow Energy Transfer in CdSe Quantum Dot Sensitized ZnO Nanowires. *J. Phys. Chem. A* **2012**, *117*, 5919−5925.
(44) Crooker, S.; Hollingsworth, J.; Tretiak, S.; Klimov, V. Spectrally Resolved Dynamics of Energy Transfer in Quantum-dot Assemblies: Towards Engineered Energy Flows in Artificial Materials. *Phys. Rev. Lett.* **2002**, *89*, 18−21.
(45) Zheng, K.; Žídek, K.; Abdellah, M.; Zhu, N.; Chábera, P.; Lenngren, N.; Chi, Q.; Pullerits, T. Directed Energy Transfer in Films of CdSe Quantum Dots: Beyond the Point Dipole Approximation. *J. Am. Chem. Soc.* **2014**, *136*, 6259−6268.
(46) Tvrdy, K.; Kamat, P. V. Substrate Driven Photochemistry of CdSe Quantum Dot Films: Charge Injection and Irreversible Transformations on Oxide Surfaces. *J. Phys. Chem. A* **2009**, *113*, 3765−3772.
(47) Wu, X.; Yeow, E. K. L. Charge-transfer Processes in Single CdSe/ZnS Quantum Dots with p-type NiO Nanoparticles. *Chem. Commun.* **2010**, *46*, 4390−4392.
(48) Collaboration: Authors and editors of the volumes III/17G-41D: *NiO: Optical Properties, Dielectric Constants*. Madelung, O.; Rössler, U.; Schulz, M. *SpringerMaterials, The Landolt-Börnstein Database*. DOI: 10.1007/10681735_518.
(49) Huang, J.; Stockwell, D.; Boulesbaa, A.; Guo, J.; Lian, T. Comparison of Electron Injection Dynamics from Rhodamine B to In_2O_3, SnO_2, and ZnO Nanocrystalline Thin Films. *J. Phys. Chem. C* **2008**, *112*, 5203−5212.
(50) Katoh, R.; Furube, A.; Hara, K.; Murata, S.; Sugihara, H.; Arakawa, H.; Tachiya, M. Efficiencies of Electron Injection from Excited Sensitizer Dyes to Nanocrystalline ZnO Films as Studied by Near-IR Optical Absorption of Injected Electrons. *J. Phys. Chem. B* **2002**, *106*, 12957.
(51) Zheng, K.; Žídek, K.; Abdellah, M.; Chábera, P.; Abd El-Sadek, M. S.; Pullerits, T. Effect of Metal Oxide Morphology on Electron Injection from CdSe Quantum Dots to ZnO. *Appl. Phys. Lett.* **2013**, *102*, 163119.
(52) Long, R.; Prezhdo, O. V. Ab Initio Nonadiabatic Molecular Dynamics of the Ultrafast Electron Injection from a PbSe Quantum Dot into the TiO2 Surface. *J. Am. Chem. Soc.* **2011**, *133*, 19240−19249.
(53) Lee, H.; Wang, M. K.; Chen, P.; Gamelin, D. R.; Zakeeruddin, S. M.; Gratzel, M.; Nazeeruddin, M. K. Efficient CdSe Quantum Dot-Sensitized Solar Cells Prepared by an Improved Successive Ionic Layer Adsorption and Reaction Process. *Nano Lett.* **2009**, *9*, 4221−4227.
(54) Hansen, T.; Žídek, K.; Zheng, K.; Abdellah, M.; Chábera, P.; Persson, P.; Pullerits, T. Orbital Topology Controlling Charge Injection in Quantum-Dot-Sensitized Solar Cells. *J. Phys. Chem. Lett.* **2014**, *5*, 1157−1162.
(55) Padilha, L. A.; Robel, I.; Lee, D. C.; Nagpal, P.; Pietrga, J. M.; Klimov, V. I. Spectral Dependence of Nanocrystal Photoionization Probability: The Role of Hot-Carrier Transfer. *ACS Nano* **2011**, *5*, 5054−5055.